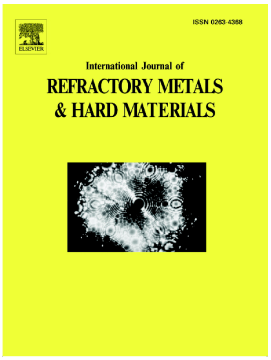

WC-base cemented carbides with partial and total substitution of Co as binder: Evaluation of mechanical response by means of uniaxial compression of micropillars

D.A. Sandoval, A. Rinaldi, A. Notargiacomo, O. Ther, J.J. Roa, L. Llanes

PII: S0263-4368(19)30420-2
DOI: https://doi.org/10.1016/j.ijrmhm.2019.105027
Article Number: 105027
Reference: RMHM 105027

To appear in: *International Journal of Refractory Metals and Hard Materials*

Received date: 1 June 2019
Revised date: 5 July 2019
Accepted date: 19 July 2019

Please cite this article as: D.A. Sandoval, A. Rinaldi, A. Notargiacomo, et al., WC-base cemented carbides with partial and total substitution of Co as binder: Evaluation of mechanical response by means of uniaxial compression of micropillars, International Journal of Refractory Metals and Hard Materials, https://doi.org/10.1016/j.ijrmhm.2019.105027

WC-base cemented carbides with partial and total substitution of Co as binder: Evaluation of mechanical response by means of uniaxial compression of micropillars

D.A. Sandoval[1,2,*], A. Rinaldi[3], A. Notargiacomo[4], O. Ther[5], J.J. Roa[1,2], L. Llanes[1,2]

[1] CIEFMA-Departament de Ciència dels Materials i Enginyeria Metal·lúrgica, EEBE, Universitat Politècnica de Catalunya, Barcelona, Spain

[2] Barcelona Research Center in Multiscale Science and Engineering, Universitat Politècnica de Catalunya, Barcelona, Spain

[3] Italian National Agency for New Technologies, Energy and Sustainable Economic Development (ENEA), Rome, Italy

[4] Institute for Photonics and Nanotechnologies – CNR (National Research Council of Italy), Rome, Italy

[5] Hyperion Materials & Technologies, Martorelles, Spain

*Corresponding author at Hyperion Materials & Technologies, Martorelles, Spain

e-mail address: daniela.sandoval@hyperionmt.com

Abstract

The influence of the chemical nature of the metallic binder on the plastic deformation of cemented carbides was studied. Three different cemented carbide grades - WC-Co, WC-CoNi and WC-NiMo - with similar microstructural characteristics (binder content and carbide grain size) were investigated. Mechanical response was evaluated by means of uniaxial compression of micropillars, and tests were carried out in-situ in a FESEM with a nanoindenter equipped with a flat-diamond punch. After uniaxial compression, inspection of deformation phenomena was done at both surface and bulk of micropillars through scanning and transmission electron microscopy, respectively. It is found that yielding phenomena and strain hardening increase as Co is totally substituted by a NiMo alloy, while contrary effect results from partial replacement of Co with Ni. Relative differences are directly linked to intrinsic ductility of the metallic phase and operative plastic deformation mechanisms. Moreover, for the three materials studied, stress-strain responses show pronounced yielding events related to glide at WC/WC interfaces. Although they are discerned at different stress levels, estimated values of sliding resistance of WC/WC boundaries are found to be alike for the three grades studied.

Keywords: cemented carbides; micromechanical testing; uniaxial compression of micropillars; TEM; plastic deformation

1. Introduction

Cemented carbides are composite materials widely used for their combination of high hardness and toughness. WC-Co is the most commonly used system due to high wettability of WC by Co during sintering and adhesion characteristics [1], leading to superior mechanical properties than other alloys. Despite this, partial or total substitution of Co as binder has been a matter of interest since few decades ago. Ni and its alloys have been used and validated as alternative binders to Co for enhancing corrosion resistance [2,3]. More recently, substitution of Co has been aimed and promoted because its classification as critical raw material by the European Union as well as hazardous substance for human health (Co powder and WC-Co dust) [4–6]. Moreover, approximately 82% of the global tungsten (also classified as critical raw element [5]) production is mined in China and prices rise constantly.

Microstructural aspects - in particular carbide contiguity and binder mean free path - affect the mechanical response of cemented carbides. For high contiguity grades, the load is supported by a continuous-like WC skeleton, through the contact between grains; thus, slip in WC or on WC/WC interfaces are dominant deformation mechanisms. As contiguity decreases, load bearing is distributed between both constitutive phases and deformation of the softer binder becomes relevant at early load stages. This takes place by slip or fcc to hcp transformation in the case of Co and Co-based alloys. Under these conditions, if the binder mean free path is sufficiently large, dislocation pile up against the carbides may occur, playing an important role in the deformation of the composite [7]. Moreover, activation of slip/twinning in metallic binder and slip in WC grains, as well as local and overall deformation extension, depend on orientation in which the load is applied [8–10].

Furthermore, interfacial strength is also expected to depend strongly on the chemical nature of the binder [11–13]. Knowledge about the nature of plastic deformation of the constitutive phases of cemented carbides is key for understanding their overall mechanical response. In this study we address this issue by attempting to understand the role of the binder phase in the mechanical response of cemented carbides. In doing so, we performed uniaxial compression of micropillars in three cemented carbide alloys: WC-Co, WC-CoNi and WC-NiMo. Deformation phenomena was studied by means of scanning and transmission electron microscopy.

2. Materials and methods

Three grades of commercial WC-base cemented carbides supplied by Hyperion Materials & Technologies were studied. The grades contain around 10 wt.% of binder and a WC mean grain size of about 1 µm. Two grades with partial and total substitution of Co as binder were selected: CoNi and NiMo, respectively. A Co-base grade was selected for comparison purposes. Microstructural characteristics of the three cemented carbides are summarized in **Table I**. Sample surfaces were polished up to mirror-like surface finish, following a 6 to 1 µm diamond-polishing protocol with a final two-step stage using colloidal silica.

Focused ion beam (FIB) was used to mill twelve micropillars of 2 µm in diameter in each sample. A two-stage milling protocol was followed. The first step was done with a dual beam Zeiss Neon 40 focused ion beam/field emission scanning electron microscope (FIB/FESEM), while the second one was conducted using a FEI-Helios Nanolab 600 dual-beam FIB. Both systems used a Ga^+ ion source operated at 30 kV. The incidence angle of the ions was 36° in both cases and the currents were 4 nA and 500 pA for the first and the second milling step, respectively. Aspect ratio of micropillars was around 4, to avoid sink-in and/or buckling of the micropillar during compression. Taper angles were kept less than 4° as usually used in annular milling [14,15]. Shape characteristics of micropillars are summarized in **Table II** and representative FESEM images are shown in **Figure 1.**

In-situ uniaxial compression of micropillars was done using a nanoindenter INSEM Nanomechanics (USA), equipped with nanopositioners SMARACT (Germany), placed inside a high-resolution field-emission-gun scanning electron microscope (FEG-SEM) LEO 35, Zeiss. Nanoindentation was carried out with a flat-diamond punch of 5 µm in nominal diameter, at a constant strain rate of 0.05 s^{-1}.

Calibration of the nanoindenter was done with a Berkovich diamond-tip on fused silica of known elastic modulus (72 GPa [16]). Tests were displacement controlled, and load (P)-displacement (h) data was continuously recorded. Stress (σ) and strain (ε) were calculated using the area at 1 µm in depth from the top of the micropillar and the total height of the micropillars, respectively. Effective elastic deformation of the indenter and the bulk material was corrected by extracting the elastic deformation of the bulk below the micropillar, using the Sneddon's approach [17,18]. Maximum loads and displacements ranges differ for each grade, because they were controlled case by case, to obtain plastic response of micropillars but avoiding catastrophic failure. Maximum load ranges were from 17 to 20 mN, 15 to 20 mN and 20 to 25 mN for WC-Co, WC-CoNi and WC-NiMo specimens respectively. Maximum displacement was fixed at 300 nm and 400 nm for WC-Co and WC-NiMo micropillars and was varied between 300 and 600 nm for WC-CoNi ones. Details of the experimental protocol followed are described elsewhere [19,20]. After uniaxial compression, deformation and/or damage features at the surface of micropillars were inspected by FESEM.

Plastic deformation mechanisms in the binder and in carbides were observed by means of transmission electron microscopy (TEM) using a JEOL JEM-2100 LaB6 unit operating at 200 kV. One micropillar of each grade was selected in which plastic deformation mechanisms were observed at the surface. To mill the TEM lamellae (with the dual beam Zeiss Neon 40 FIB/FESEM), we selected one micropillar of each grade in which plastic deformation mechanisms were evidenced at the surface. Prior to milling the lamellae, a Carbon-Platinum (C:Pt) layer of around 2 µm in thickness was deposited in all the surface of the micropillars to avoid Ga^+ interaction with the samples. Once the lamellae were extracted from the sample and placed in a Cu grid, they were thinned up to around 60 nm of thickness at 30 kV, and finally polished with a 5 kV beam energy to reduce the amorphous layer and up to 60 nm of thickness.

3. Results and discussion

3.1 Mechanical response after uniaxial compression of micropillars

Stress-strain (σ-ε) curves plotted from load-displacement (P-h) data recorded for each material studied are shown in **Figure 2**. In general, relatively high yield stresses are achieved during micropillar compression for the three cemented carbide grades. Considering their intrinsic composite nature and inter-dispersed phase network arrangement, these findings highlight the strength of phase boundaries in impeding dislocation motion as well as the effective constraining effect of the hard ceramic phase on the soft metallic one [21]. For the three materials a strain-hardening effect is depicted from the loading curve. Strain hardening rate (SHR) is higher for WC-NiMo specimens than for WC-Co and WC-CoNi ones. Work hardening is expected to decrease as the amount of Ni increases in a Co-Ni alloy [22], in agreement with the response evidenced in **Figure 2**. Meanwhile, extremely high SHRs found for WC-NiMo specimens should be ascribed to solid-solution strengthening, expected to be very effective in Ni-Mo alloys because size and valence differences together with electronic interaction between solute and solvent as well as changes in stacking fault energy values [23–27]. This is supported by the fact that SHR values are higher (about 7 GPa) than those reported as typical bulk values for stage II work hardening (between 2.6 and 5.2 GPa) for Ni [28]. Nevertheless, SHR size-effects due to localized binder pools available for deformation could also be recalled for explaining the discerned strain-hardening response.

Plastic deformation and possible activation of slip phenomena are depicted as strain bursts in the loading curve of grades containing Co- and CoNi- based metallic binders, before a pronounced yielding event occurred (**Figure 2**). Displacement magnitude at each strain burst seems to be

variable. Although uniaxial compression tests are carried upon micropillars representative of the composite material, the strain state is not completely independent of local stretch or rotational plastic gradients at binder regions, as a consequence of the disposal of surrounding WC particles, i.e. constraining effect of WC particles [29]. Moreover, distribution of phases is random in each micropillar; thus, orientation of the applied load is expected to affect the response of the binder, as some crystal orientations are not only more susceptible to initiate or activate dislocation motion than others but also to exhibit different SHRs [30]. It could explain, at least partly, the variation on the mechanical response of individual micropillars evidenced for a given grade. This fact is even more complex to analyse in the case of Co, as type and reaction of dislocations also differ in fcc and hcp Co [31].

Regarding partial substitution of Co by Ni, as seen in **Figure 3**, strain bursts at a defined strain level occurred at lower stresses for WC-CoNi micropillars than for WC-Co ones. It could be rationalized in terms of the intrinsic ductility of the binder which appears to increase with addition of Ni, probably because of the depletion of fcc to hcp martensitic transformation, known to reduce ductility of the Co binder [22]. Furthermore, variation in stress magnitude linked to strain bursts in both WC-Co and WC-CoNi composites during loading may be also size-affected, because sample dimension and mean free path limit the length scales available for plasticity [21]. Within this context, strain bursts occurring at stress levels from 1 to 4 GPa are attributed to plastic flow and evolving deformation of metallic binder. The thinner the binder layers, i.e. more constrained, the higher the stress value at which such abrupt plastic events are evidenced. On the other hand, strain bursts observed at even higher stress levels are rather associated with slip activity within WC particles and WC/WC interface phenomena [20].

Different from the mechanical response exhibited by Co- and CoNi- based grades, no strain bursts were depicted in the loading curves of micropillars of WC-NiMo grade. Such experimental fact together to the quite high yield stresses measured for WC-NiMo specimens should be linked to low dislocation density or even dislocation starvation during deformation of the material. Possible reasons behind this deformation scenario would be effective solid solution strengthening of Ni by Mo alloying, including changes in stacking fault energy. Under these conditions, high stresses are needed to nucleate dislocations for plasticity to proceed [32]. However, once stress levels for irreversible deformation were achieved (above 3.5 GPa), most of the pillars did show a well-defined and pronounced yielding event. Very interesting, these plateau-like phenomena in WC-NiMo micropillars were similar to those evidenced in WC-Co and WC-NiCo specimens, but without any preceding strain burst event.

Representative pronounced yielding events - causing a strain of around 1% for WC-Co and 3% for WC-CoNi and WC-NiMo but taking place a quite similar stress levels - are depicted in **Figure 4** for the three materials. σ-ε curves for these events are also shown in this figure. From SEM imaging of the surface of these three micropillars, we observed a common deformation mechanism: glide at WC/WC interfaces (**Figure 4**). We then estimated shear stresses (τ_s) for each case by assuming that plateau-like yielding event for each micropillar was associated with prominent glide discerned at WC/WC interfaces [33,34]. To do so, we measured the glide angle (θ) directly from SEM images, discarding the influence of a possible variation due to image perspective (see scheme in **Figure 4**). The angles determined were 33, 35 and 56 degrees for Co, CoNi and NiMo grades, respectively. Load was taken directly from the load-displacement data. Meanwhile, possible effects related to taper angle or orientation of WC particles were either disregarded or not accounted. Relatively similar interfacial strength values - around 2.0 GPa - were obtained for the three grades. Such values are within the lower bound range of shear stresses (between 2 and 7 GPa) required for WC/WC

interfacial displacement, as estimated from molecular dynamics simulation of WC/WC grain boundary sliding resistance at room temperature [35]. In the case of WC-Co, the event is not as pronounced as for the other two alloys, possibly because interfacial strength may indeed be higher than the estimated one. Studies have shown that concentration of WC/WC grain boundary type is constant and it does not depend on any microstructural feature, rather than the starting materials in which 90°/[10-10] grain boundaries are abundant [11]. In this sense, glide at WC/WC interfaces could depend on the angle in which WC/WC interfaces are with respect to the applied load. This is observed in **Figure 2**, where σ-ε curves for WC-NiMo exhibit the same shape hinting to a first event of glide between WC particles at different stresses (due to different θ angles), followed by other mechanisms of deformation activated, such as plastic deformation of WC particles and decohesion. In the case of WC-Co and WC-CoNi composites, other deformation mechanisms are activated at the beginning of the load (plastic flow and deformation of the binder); thus, local arrangement of particles may change, promoting the occurrence of other deformation mechanisms, besides WC/WC gliding.

3.2 Plastic deformation of binder and WC

TEM images of micropillars are shown in **Figures 5** to **7**. Deformation of Co binder (**Figure 5 b** and **c**) is seen as thin lamellae (laths) of hcp material. Stacking faults (SFs) present in the material before deformation increase during compression and coalesce to form hcp lamellae [36]. It is well known that the allotropic transformation of Co from fcc to hcp occurs preferably by a martensitic reaction. However, W and C dissolved in Co may retard this martensitic transformation and restrictions imposed by WC skeleton may have similar effect [36]. In addition, fcc to hcp transformation of Co may also be induced by FIB milling [37]. Thus, deformation observed should be a combination of

initial hcp to fcc ratio and fcc to hcp transformation induced by sample preparation and uniaxial compression.

As Co is substituted by 25 wt.% of Ni, the predominant deformation mechanism within the binder shifts from fcc-hcp martensitic transformation of Co, towards planar slip (**Figure 6 b** and **c**), in agreement with Vasel *et al's* findings [22]. However, clear stacking faults (SFs) were not evidenced. Considering that nickel exhibits a stacking fault energy (SFE) significantly higher than cobalt [22,38,39] and that SFE of nickel-cobalt alloys increases as Ni/Co ratio rises [40], it could be speculated that SFE for the CoNi alloy here studied (Co/Ni ratio of 80/20) is relatively high. It would then result in either extremely narrow or simply absent SFs, and suppression of fcc to hcp phase transformation. Meanwhile, dislocation arrays were heterogeneously distributed within binder regions, possibly as direct consequence of a similarly inhomogeneous distribution of stress and strain, due to the differences in stiffness of the constitutive phases of the composite.

For NiMo binder, deformation mechanisms consist preferentially of simple slip by dislocation motion, as depicted in **Figure 7 b** and **c**. Dislocation density seems to be lower than for the other specimens studied. Such experimental fact, together with the relatively limited TEM inspection conducted in this study does not allow to provide further details in terms of slip mode (either wavy or planar) for this metallic alloy. Amorphization signs due to Ga^{+} ions implantation can be seeing as "salt and pepper" features. This is an artifact created during TEM sample preparation and not during compression [30,41–43]. However, dislocations can be distinguished as defined lines. Those dislocations in NiMo binder are either created during plastic deformation or present in the initial dislocation density. Furthermore, multiplication of dislocations in Ni is affected by free surfaces setting distances for flow [44]. In other words, multiplication of dislocations is restricted by binder

mean free path. Therefore, their distribution will change as the total volume of the sample, i.e. binder pools, changes.

Signs of plastic deformation of WC within micropillars are discerned in **Figure 4**. Such slip lines were not observed in the ceramic phase in all micropillars, possibly due to distinct relative crystal orientation with respect to applied load direction [10]. On the other hand, SFs and dislocations are observed in WC in TEM images, especially in WC-Co and WC-CoNi grades (see **Figures 5 d** and **6 d**). Bent dislocations - called bent dislocations - are the predominant deformation mechanism of plastic deformation observed in WC within the NiMo grade (see **Figure 7 d**). Here, carbide is observed to deform through a gliding mechanism [36].

Results show that plastic deformation of the binder dominates early stages of plastic deformation of cemented carbides, i.e. intrinsic plastic deformation phenomena of the metallic alloy governs the response of the composite at initial loads. In this sense, fcc to hcp martensitic transformation of Co has a direct effect on the strain-hardening rates which is higher than for the material with partial substitution of Co by Ni. In the WC-CoNi grade, planar slip within binder pools and dislocation starvation at binder free surfaces, governs the plastic deformation. The evidence of these mechanisms, instead of fcc to hcp transformation of Co, would indicate a lower energy requirement for the former than for the latter. Finally, total substitution of Co by Ni-alloy binder – as it is the case for this study - assumes that plastic deformation occurs only by dislocation-dislocation interaction and dislocation starvation, which is completely dependent on binder mean free path and in small samples, on areas where free surfaces of binder are available, from which the dislocations can exit the material. Once the binder reaches its maximum ability to deform plastically due to its intrinsic strain range and the constraint imposed by WC particles, interfacial strength plays an important role in the overall mechanical response of cemented carbides. In this regard, interfacial strength of the

three cemented carbide grades studied, assessed based on sliding resistance of WC/WC boundaries, is relatively similar with values around 2 GPa.

4. Conclusions

In the present study the role of the binder in the plastic deformation of cemented carbides was studied. In doing so, local plastic deformation and damage phenomena of WC-base cemented carbides, with Co and partial and total substitution of Co as binder, were evaluated by means of uniaxial compression of micropillars. The following conclusions may be drawn:

1. At early stages of loading, plastic activity within the binder governs irreversible deformation of cemented carbide micropillars. Such plastic deformation is intrinsic to the chemical nature of the binder. In this sense, yielding stresses and strain hardening rates (SHR) decrease as Co is partially substituted by Ni and increase with full substitution of Co by a NiMo alloy.

2. Occurrence of strain bursts, and stress/strain levels at which they emerge for tested micropillars can be attributed to plastic deformation capability of binder regions. Hence, frequency and magnitude of these abrupt plasticity effects will be dependent on intrinsic ductility (phase transformation, slip activation and/or dislocation density during deformation) of the binder as well as on constraining effects imposed by the surrounding WC particles.

3. As strain imposed and resulting stress rise, glide at WC/WC interfaces shows up as a plateau-like yielding event. The stress levels at which this deformation mechanism is evidenced depends strongly on the distribution of phases, and particularly on the orientation of WC particles with respect to the applied load. Nevertheless, gliding resistance of WC/WC boundaries estimated (about 2 GPa) is quite similar for the three cemented carbides studied.

4. Plastic deformation mechanisms change from fcc-hcp transformation to dislocation-mediated activity as Co is substituted by Ni. However, dislocation density and corresponding plastic deformation is also affected by Mo-alloying effects on Ni, in agreement with the pronounced strengthening measured in the stress-strain response of WC-NiMo grade.

Acknowledgements

This investigation was partially supported by the Spanish Ministerios de Economía y Competitividad MINECO y de Ciencia, Innovación y Universidades MICINN - FEDER through grants MAT2015- 70780-C4-3-P and PGC2018-096855-B-C41 respectively, and by the industry-university collaborative program between Hyperion Materials & Technologies and UPC. D.A. Sandoval would like to acknowledge the funding received by the COST Action CA15102 "Solutions for Critical Raw Materials under Extreme Conditions" for a Short Term Scientific Mission at ENEA, and Dr. Trifon Trifonov at Barcelona Research Center in Multiscale Science and Engineering, for FIB milling of micropillars and TEM lamellae preparation.

References

[1] H.E. Exner, Physical and chemical nature of cemented carbides, Int. Mater. Rev. 4 (1979) 1149–73. doi:10.1179/imtr.1979.24.1.149.

[2] W.J. Tomlinson, C.R. Linzell, Anodic polarization and corrosion of cemented carbides with cobalt and nickel binders, J. Mater. Sci. 23 (1988) 914–918. doi:10.1007/BF01153988.

[3] E.J. Wentzel, C. Allen, The erosion-corrosion resistance of tungsten-carbide hard metals, Int. J. Refract. Met. Hard Mater. 15 (1997) 81–87. doi:10.1016/S0263-4368(96)00016-9.

[4] B. Gries, L.J. Prakash, Acute inhalation toxicity by contact corrosion - The case of WC-Co, Euro PM 2007, Powder Metall. World Congr. Exhib. 2007 Oct 15-17; Toulouse. Vol. 1 (2007) 189–196.

[5] M. Grilli, T. Bellezze, E. Gamsjäger, A. Rinaldi, P. Novak, S. Balos, R. Piticescu, M. Ruello, M.L. Grilli, T. Bellezze, E. Gamsjäger, A. Rinaldi, P. Novak, S. Balos, R.R. Piticescu, M.L. Ruello, Solutions for Critical Raw Materials under Extreme Conditions: A Review, Materials (Basel). 10 (2017) 285. doi:10.3390/ma10030285.

[6] U.S. Department of Health and Human Services, National Toxicology Program (NTP), (n.d.). http://ntp.niehs.nih.gov/ (accessed April 4, 2016).

[7] V.B. John, V.B. John, Elastic and Plastic Behaviour, Introd. to Eng. Mater. 9 (2015) 73–100. doi:10.1007/978-1-349-17190-3_5.

[8] G.Y. Chin, W.F. Hosford, D.R. Mendorf, Accommodation of constrained deformation in f.c.c. metals by slip and twinning, Proc. R. Soc. A Math. Phys. Eng. Sci. (1969) 433–456. doi:10.1098/rspa.1969.0051.

[9] B. Roebuck, P. Klose, K.P. Mingard, Hardness of hexagonal tungsten carbide crystals as a

function of orientation, Acta Mater. 60 (2012) 6131–6143. doi:10.1016/j.actamat.2012.07.056.

[10] T. Csanádi, M. Bľanda, A. Duszová, N.Q. Chinh, P. Szommer, J. Dusza, Deformation characteristics of WC micropillars, J. Eur. Ceram. Soc. 34 (2014) 4099–4103. doi:10.1016/j.jeurceramsoc.2014.05.045.

[11] C.S. Kim, T.R. Massa, G.S. Rohrer, Interface character distributions in WC-Co composites, J. Am. Ceram. Soc. 91 (2008) 996–1001. doi:10.1111/j.1551-2916.2007.02226.x.

[12] X. Song, Y. Gao, X. Liu, C. Wei, H. Wang, W. Xu, Effect of interfacial characteristics on toughness of nanocrystalline cemented carbides, Acta Mater. 61 (2013) 2154–2162. doi:10.1016/J.ACTAMAT.2012.12.036.

[13] X. Liu, X. Song, H. Wang, X. Liu, X. Wang, G. Guo, Preparation and mechanisms of cemented carbides with ultrahigh fracture strength, J. Appl. Crystallogr. 48 (2015) 1254–1263. doi:10.1107/S1600576715012832.

[14] H. Zhang, B.E. Schuster, Q. Wei, K.T. Ramesh, The design of accurate micro-compression experiments, Scr. Mater. 54 (2006) 181–186. doi:10.1016/j.scriptamat.2005.06.043.

[15] J.M. Wheeler, J. Michler, Elevated temperature, nano-mechanical testing in situ in the scanning electron microscope, Rev. Sci. Instrum. 84 (2013) 045103. doi:10.1063/1.4795829.

[16] W.C. Oliver, G.M. Pharr, An improved technique for determining hardness and elastic modulus using load and displacement sensing indentation experiments, J. Mater. Res. 7 (1992) 1564–1583. doi:10.1557/jmr.1992.1564.

[17] C.A. Volkert, E.T. Lilleodden, Size effects in the deformation of sub-micron Au columns, Philos. Mag. 86 (2006) 5567–5579. doi:10.1080/14786430600567739.

[18] B. Poon, D. Rittel, G. Ravichandran, An analysis of nanoindentation in linearly elastic solids,

Int. J. Solids Struct. 45 (2008) 6018–6033. doi:10.1016/j.ijsolstr.2008.07.021.

[19] D.A. Sandoval, A. Rinaldi, J.M. Tarragó, J.J. Roa, J. Fair, L. Llanes, Scale effect in mechanical characterization of WC-Co composites, Int. J. Refract. Met. Hard Mater. 72 (2018) 157–162. doi:10.1016/j.ijrmhm.2017.12.029.

[20] D.A. Sandoval, A. Rinaldi, A. Notargiacomo, O. Ther, E. Tarrés, J.J. Roa, L. Llanes, Influence of specimen size and microstructure on uniaxial compression of WC-Co micropillars, Ceram. Int. 45 (2019) 15934–15941. doi:10.1016/j.ceramint.2019.05.102.

[21] J.J. Roa, E. Jiménez-Piqué, J.M. Tarragó, D.A. Sandoval, A. Mateo, J. Fair, L. Llanes, Hall-Petch strengthening of the constrained metallic binder in WC–Co cemented carbides: Experimental assessment by means of massive nanoindentation and statistical analysis, Mater. Sci. Eng. A. (2016). doi:10.1016/j.msea.2016.09.020.

[22] C.H. Vasel, A.D. Krawitz, E.F. Drake, E.A. Kenik, Binder deformation in WC-(Co, Ni) cemented carbide composites, Metall. Trans. A. 16 (1985) 2309–2317. doi:10.1007/BF02670431.

[23] L. Deléhouzée, A. Deruyttere, The stacking fault density in solid solutions based on copper, silver, nickel, aluminium and lead, Acta Metall. 15 (1967) 727–734. doi:10.1016/0001-6160(67)90353-7.

[24] B. Gan, S. Tin, Assessment of the effectiveness of transition metal solutes in hardening of Ni solid solutions, Mater. Sci. Eng. A. 527 (2010) 6809–6815. doi:10.1016/J.MSEA.2010.06.071.

[25] K.K. Mehta, P. Mukhopadhyay, R.K. Mandal, A.K. Singh, Microstructure, texture, and orientation-dependent flow behavior of binary Ni-16Cr and Ni16Mo solid solution alloys, Metall. Mater. Trans. A. 46 (2015) 3656–3669.

[26] A. Pathak, A.K. Singh, A. Pathak, A.K. Singh, Mechanical properties of Ni-based solid solution alloys: A first principles study, J. Appl. Res. Technol. 15 (2017) 449–453. doi:10.1016/j.jart.2017.05.006.

[27] W. Zhao, W. Li, Z. Sun, S. Gong, L. Vitos, Tuning the plasticity of Ni-Mo solid solution in Ni-based superalloys by ab initio calculations, Mater. Des. 124 (2017) 100–107. doi:10.1016/J.MATDES.2017.03.057.

[28] A. Seeger, Plasticity of crystals, in: Handb. Der Phys., Berlin, 1958: pp. 1–28.

[29] D.E. Hurtado, M. Ortiz, Surface effects and the size-dependent hardening and strengthening of nickel micropillars, J. Mech. Phys. Solids. 60 (2012) 1432–1446. doi:10.1016/j.jmps.2012.04.009.

[30] C.P. Frick, B.G. Clark, S. Orso, A.S. Schneider, E. Arzt, Size effect on strength and strain hardening of small-scale [1 1 1] nickel compression pillars, Mater. Sci. Eng. A. 489 (2008) 319–329. doi:10.1016/j.msea.2007.12.038.

[31] Q. Feng, X. Song, H. Xie, H. Wang, X. Liu, F. Yin, Deformation and plastic coordination in WC-Co composite — Molecular dynamics simulation of nanoindentation, Mater. Des. 120 (2017) 193–203. doi:10.1016/j.matdes.2017.02.010.

[32] Z.W. Shan, R.K. Mishra, S.A. Syed Asif, O.L. Warren, A.M. Minor, Mechanical annealing and source-limited deformation in submicrometre-diameter Ni crystals, Nat. Mater. 7 (2008) 115–119. doi:10.1038/nmat2085.

[33] C. Shih, Y. Katoh, K.J. Leonard, H.B.E. Lara-curzio, Determination of interfacial mechanical properties of ceramic composites by the compression of micro-pillar test specimens, J. Mater. Sci. (2013) 5219–5224. doi:10.1007/s10853-013-7311-z.

[34] M.C. Liu, J.C. Huang, Y.T. Fong, S.P. Ju, X.H. Du, H.J. Pei, T.G. Nieh, Assessing the interfacial strength of an amorphous–crystalline interface, Acta Mater. 61 (2013) 3304–3313. doi:10.1016/j.actamat.2013.02.019.

[35] M.V.G. Petisme, M.A. Gren, G. Wahnström, Molecular dynamics simulation of WC/WC grain boundary sliding resistance in WC–Co cemented carbides at high temperature, Int. J. Refract.

Met. Hard Mater. 49 (2015) 75–80. doi:10.1016/J.IJRMHM.2014.07.037.

[36] V.K. Sarin, T. Johannesson, On the Deformation of WC–Co Cemented Carbides, Met. Sci. 9 (2010) 472–476. doi:10.1179/030634575790444531.

[37] H.G. Jones, A.P. Day, D.C. Cox, Electron backscatter diffraction studies of focused ion beam induced phase transformation in cobalt, Mater. Charact. 120 (2016) 210–219. doi:10.1016/j.matchar.2016.09.004.

[38] L. Rémy, A. Pineau, Twinning and strain-induced f.c.c. → h.c.p. transformation on the mechanical properties of Co□Ni□Cr□Mo alloys, Mater. Sci. Eng. 26 (1976) 123–132. doi:10.1016/0025-5416(76)90234-2.

[39] L. Remy, Kinetics of f.c.c. deformation twinning and its relationship to stress-strain behaviour, Acta Metall. 26 (1978) 443–451. doi:10.1016/0001-6160(78)90170-0.

[40] B.E.P. Beeston, I.L. Dillamore, R.E. Smallman, The Stacking-Fault Energy of Some Nickel-Cobalt Alloys, Met. Sci. J. 2 (1968) 12–14. doi:10.1179/030634568790443468.

[41] T. Ishitani, H. Tsuboi, T. Yaguchi, H. Koike, Transmission Electron Microscope Sample Preparation Using a Focused Ion Beam, J. Electron Microsc. (Tokyo). 43 (1994) 322–326. doi:10.1093/oxfordjournals.jmicro.a051119.

[42] D. Larson, D. Foord, A. Petford-Long, T. Anthony, I. Rozdilsky, A. Cerezo, G. Smith, Focused ion-beam milling for field-ion specimen preparation: preliminary investigations, Ultramicroscopy. 75 (1998) 147–159. doi:10.1016/S0304-3991(98)00058-8.

[43] L.A. Giannuzzi, Introduction to Focused Ion Beams: Instrumentation, Theory, Techniques and Practice, Springer Science & Business Media, 2006.

[44] D.M. Dimiduk, M.D. Uchic, T.A. Parthasarathy, Size-affected single-slip behavior of pure nickel microcrystals, Acta Mater. 53 (2005) 4065–4077. doi:10.1016/j.actamat.2005.05.023.

List of tables

Table I. Binder content and composition, WC mean grain size (d_{WC}), binder mean free path (λ_{binder}), WC contiguity (C_{WC}) and hardness (HV_{30}) for the cemented carbide grades studied.

Grade	Binder	d_{WC} (μm)	λ_{binder} (μm)	C_{WC} (μm)	HV_{30} (GPa)
WC-Co	11 wt.% Co	1.1 ± 0.7	0.4 ± 0.3	0.4 ± 0.1	12.8 ± 0.2
WC-CoNi	8 wt.% Co – 2wt.% Ni	1.0 ± 0.8	0.4 ± 0.3	0.4 ± 0.1	12.3 ± 0.1
WC-NiMo	9 wt.% Ni – 1 wt.% Mo	1.0 ± 0.8	0.4 ± 0.3	0.4 ± 0.1	11.7 ± 0.2

Table II. Shape and size characteristics of micropillars: micropillars diameter (d_{pillar}), aspect ratio of micropillars (L_{pillar}/d_{pillar}) and taper angle (α), milled in each cemented carbide grade studied.

Grade	d_{pillar} (μm)	L_{pillar}/d_{pillar}	α (deg.)
WC-Co	2.0 ± 0.0	3.7 ± 0.1	3.2 ± 0.5
WC-CoNi	2.0 ± 0.0	3.6 ± 0.1	3.1 ± 0.3
WC-NiMo	2.0 ± 0.1	3.8 ± 0.3	3.4 ± 0.4

List of figures

Figure 1. FESEM images of representative micropillars milled in a) WC-Co, b) WC-CoNi and c) WC-NiMo cemented carbide grades studied.

Figure 2. Stress-strain (σ-ε) curves plotted from load-displacement (*P*-*h*) data recorded continuously during uniaxial compression of micropillars in each cemented carbide grade studied.

Figure 3. Strain burst events detected during loading for each grade studied.

Figure 4. a) Stress-strain (σ-ε) curves of one micropillar for each cemented carbide grade, in which a single strain event was detected during uniaxial compression test; b), c) and d) FESEM images of surface of micropillars in WC-Co, WC-CoNi and WC-NiMo respectively, after uniaxial compression showing a common glide between at WC/WC interfaces. A schematic representation of parameters used to calculate shear stress at the interfaces is shown in a), where σ is the stress at which the single strain event was detected, θ is the interface angle, A is the area at the surface of the micropillar, and τs is the shear stress defined as $\sigma \cdot Sen\theta \cdot Cos\theta$.

Figure 5. TEM images of one micropillar of WC-Co grade: a) dark field image of the micropillar in which darker phase corresponds to WC and lighter phase corresponds to Co binder; detail of b) hcp lamellae (arrowed) and c) planar slip (arrowed) evidenced in Co binder after deformation; and d) stacking faults and dislocations in WC.

Figure 6. TEM images of one micropillar of WC-CoNi grade: a) dark field image of the micropillar in which lighter phase corresponds to WC and darker phase corresponds to CoNi binder; b) and c) detail of planar slip in CoNi binder after deformation; and d) stacking faults and dislocations in WC.

Figure 7. TEM images of one micropillar of WC-NiMo grade: a) dark field image of the micropillar in which lighter phase corresponds to WC and darker phase corresponds to NiMo binder; b) and c) detail of dislocations in NiMo binder after deformation; and d) bent dislocations in WC.

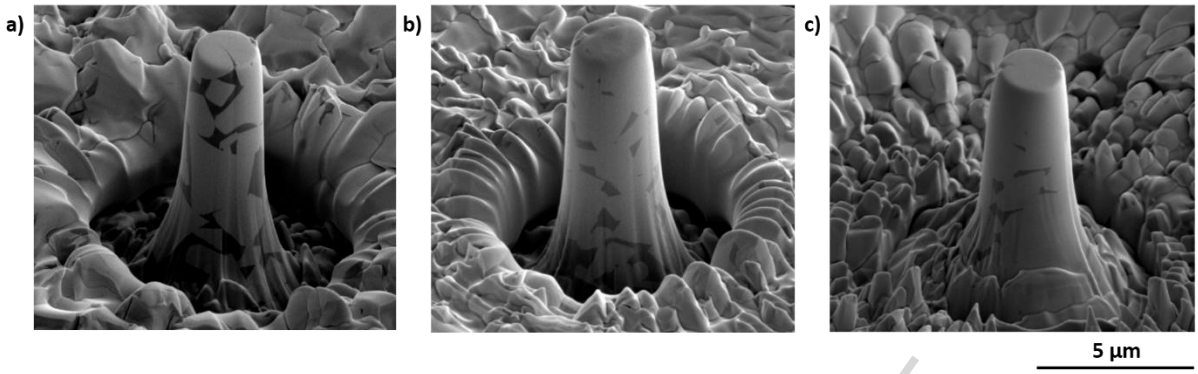

Figure 1. FESEM images of representative micropillars milled in a) WC-Co, b) WC-CoNi and c) WC-NiMo cemented carbide grades studied.

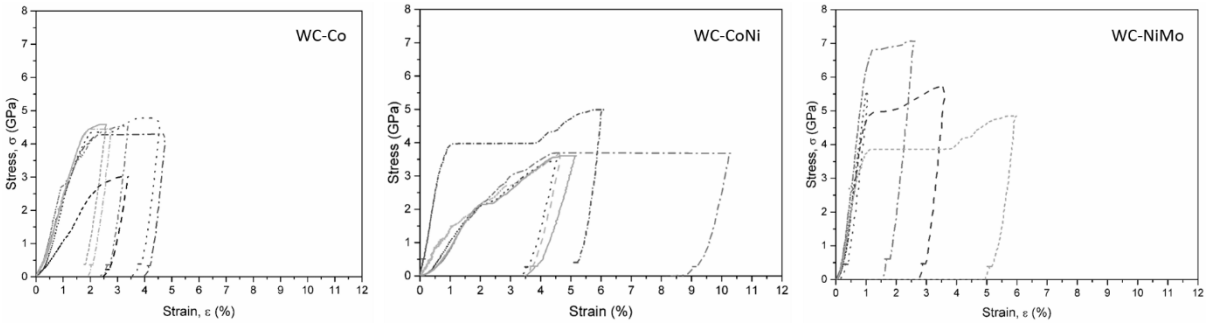

Figure 2. Stress-strain (σ-ε) curves plotted from load-displacement (*P*-*h*) data recorded continuously during uniaxial compression of micropillars in each cemented carbide grade studied.

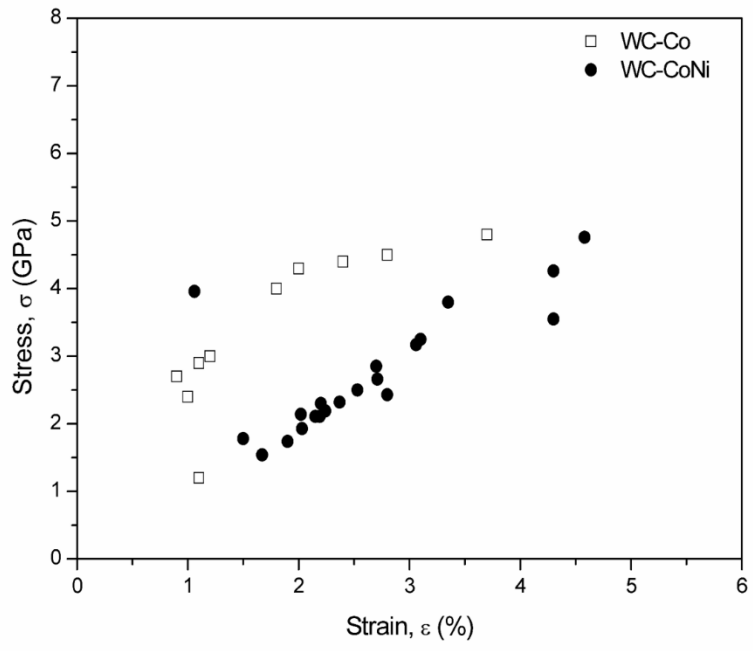

Figure 3. Strain burst events detected during loading for each grade studied.

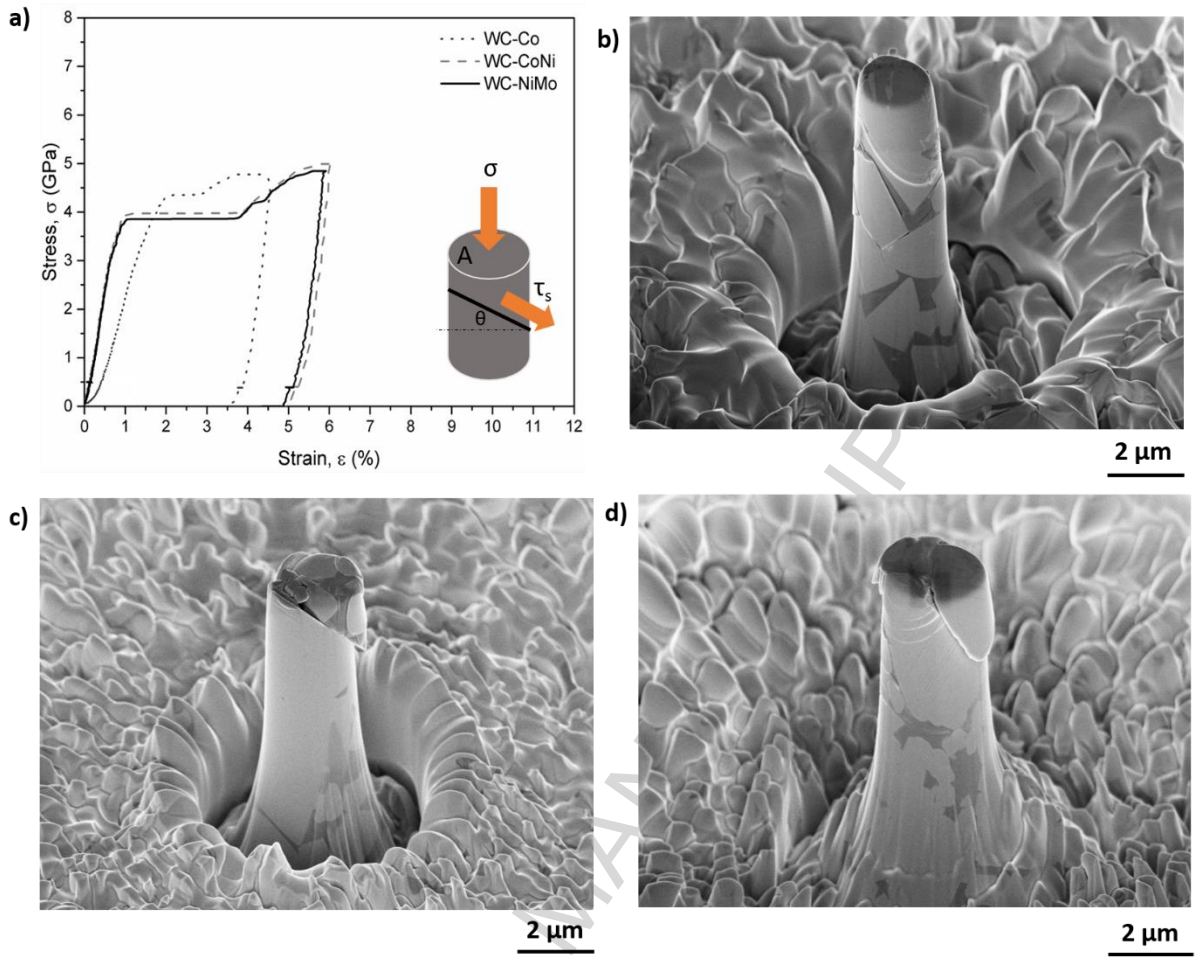

Figure 4. a) Stress-strain (σ-ε) curves of one micropillar for each cemented carbide grade, in which a single strain event was detected during uniaxial compression test; b), c) and d) FESEM images of surface of micropillars in WC-Co, WC-CoNi and WC-NiMo respectively, after uniaxial compression showing a common glide between at WC/WC interfaces. A schematic representation of parameters used to calculate shear stress at the interfaces is shown in a), where σ is the stress at which the single strain event was detected, θ is the interface angle, A is the area at the surface of the micropillar, and τ_s is the shear stress defined as $\sigma \cdot Sen\theta \cdot Cos\theta$.

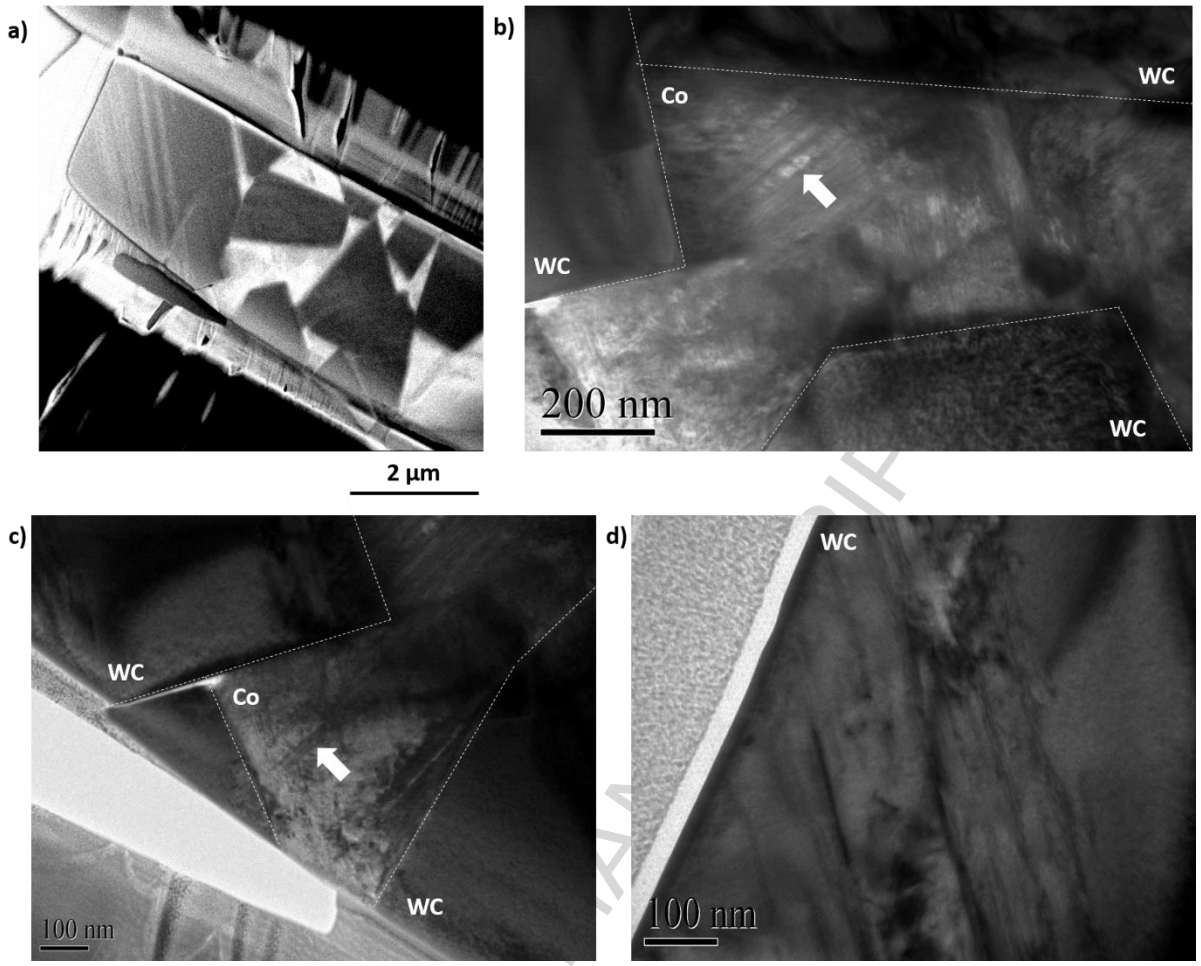

Figure 5. TEM images of one micropillar of WC-Co grade: a) dark field image of the micropillar in which darker phase corresponds to WC and lighter phase corresponds to Co binder; detail of b) hcp lamellae (arrowed) and c) planar slip (arrowed) evidenced in Co binder after deformation; and d) stacking faults and dislocations in WC.

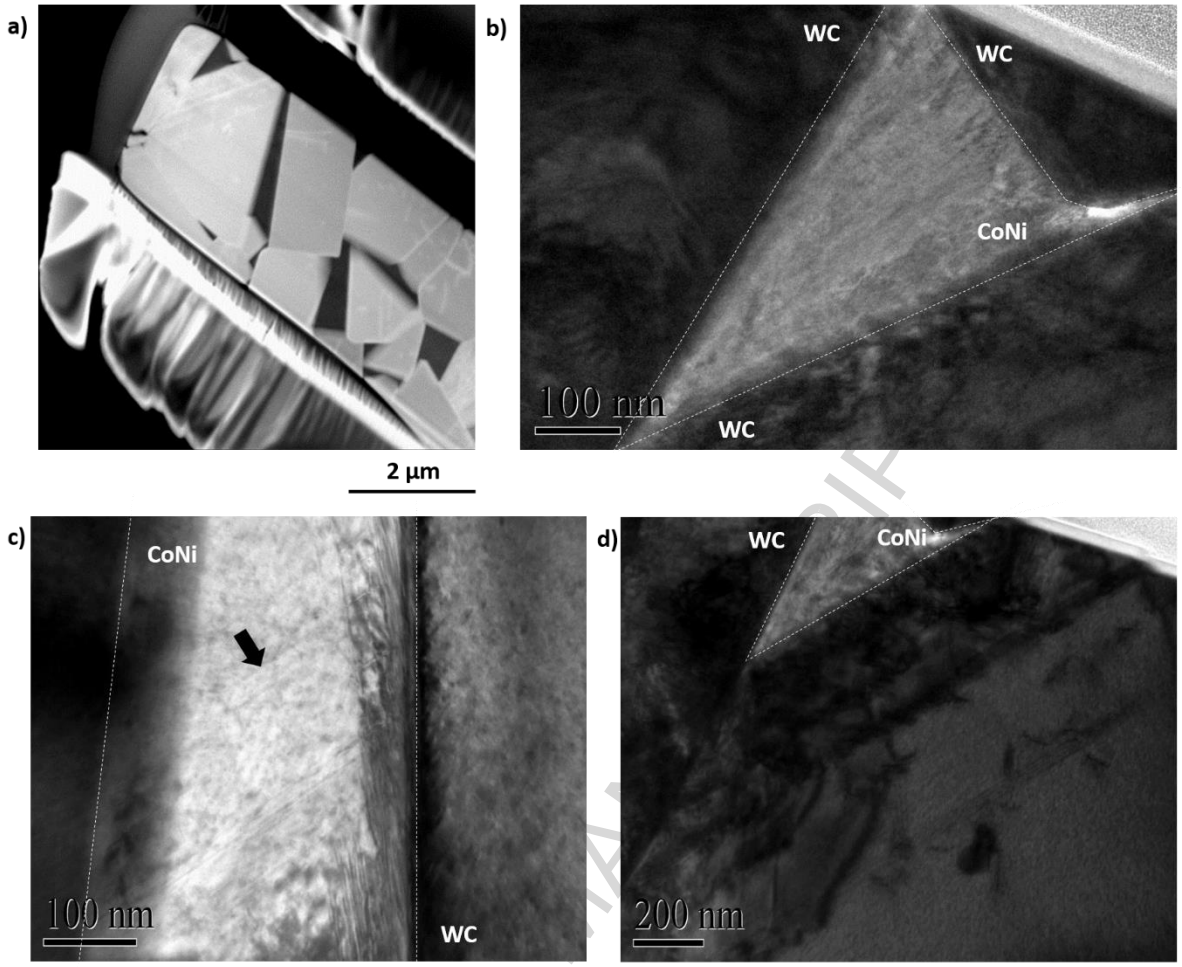

Figure 6. TEM images of one micropillar of WC-CoNi grade: a) dark field image of the micropillar in which lighter phase corresponds to WC and darker phase corresponds to CoNi binder; b) and c) detail of planar slip in CoNi binder after deformation; and d) stacking faults and dislocations in WC.

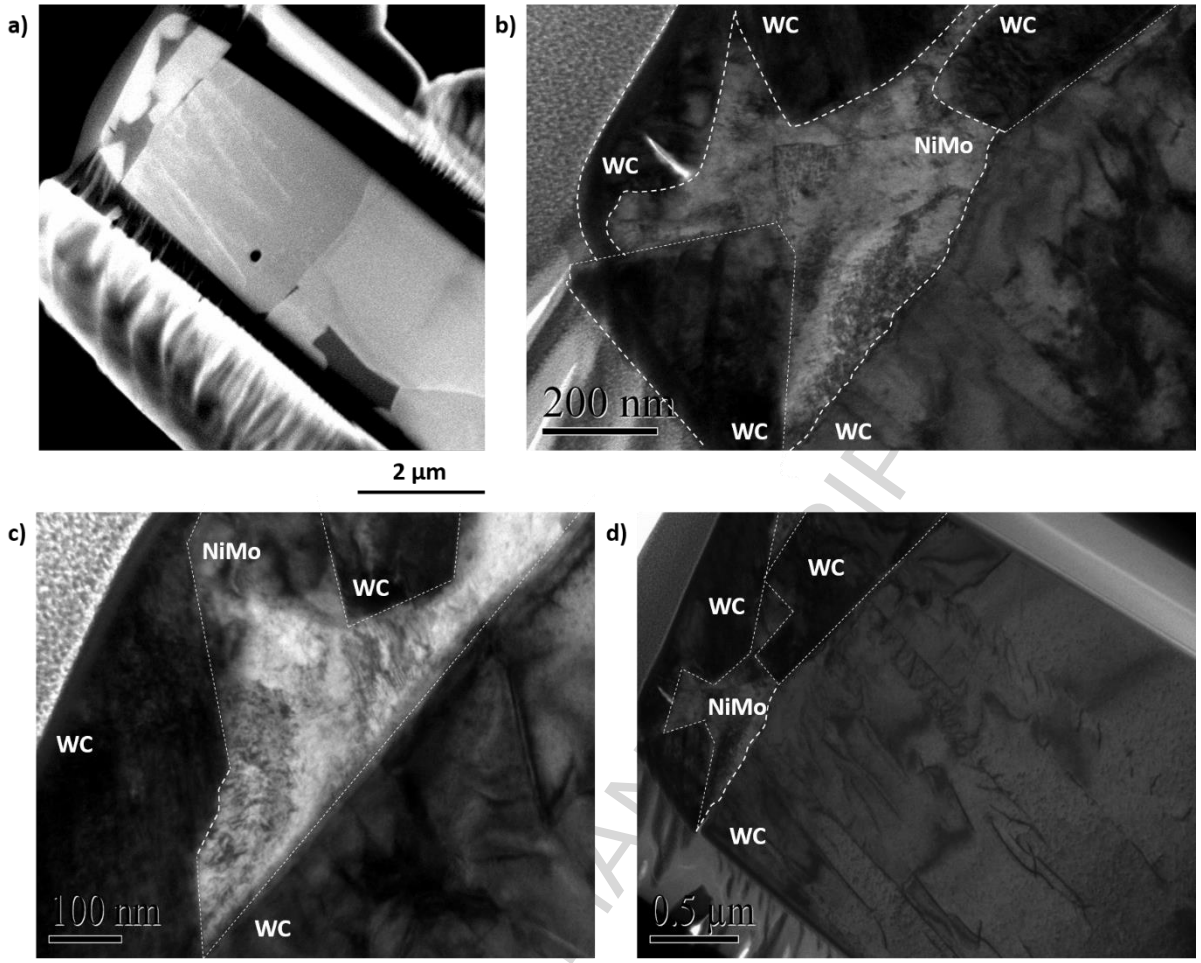

Figure 7. TEM images of one micropillar of WC-NiMo grade: a) dark field image of the micropillar in which lighter phase corresponds to WC and darker phase corresponds to NiMo binder; b) and c) detail of dislocations in NiMo binder after deformation; and d) bent dislocations in WC.

- Early irreversible deformation is linked to plastic activity within metallic binder
- Plastic deformation of binder intrinsically depends on its chemical nature
- Deformation ability of binder is extrinsically affected by constraining from WC
- Binder chemical nature does not seem to affect WC/WC gliding resistance

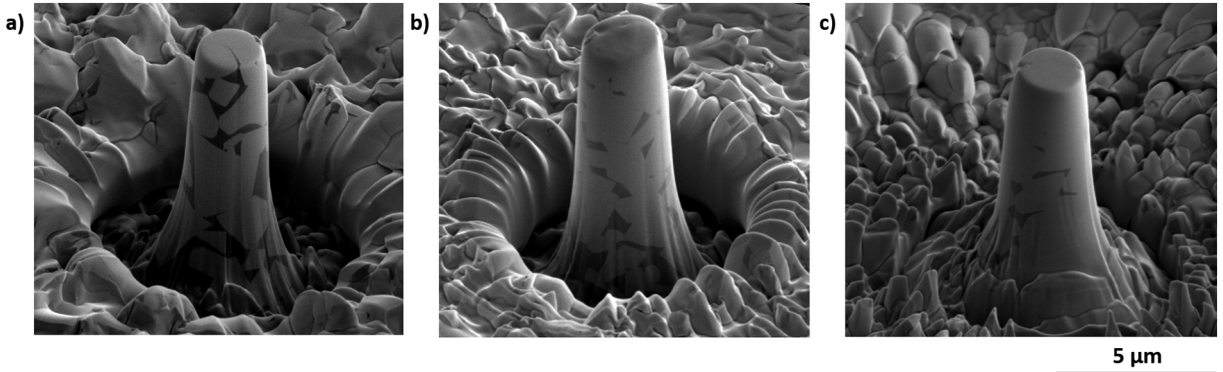

Figure 1

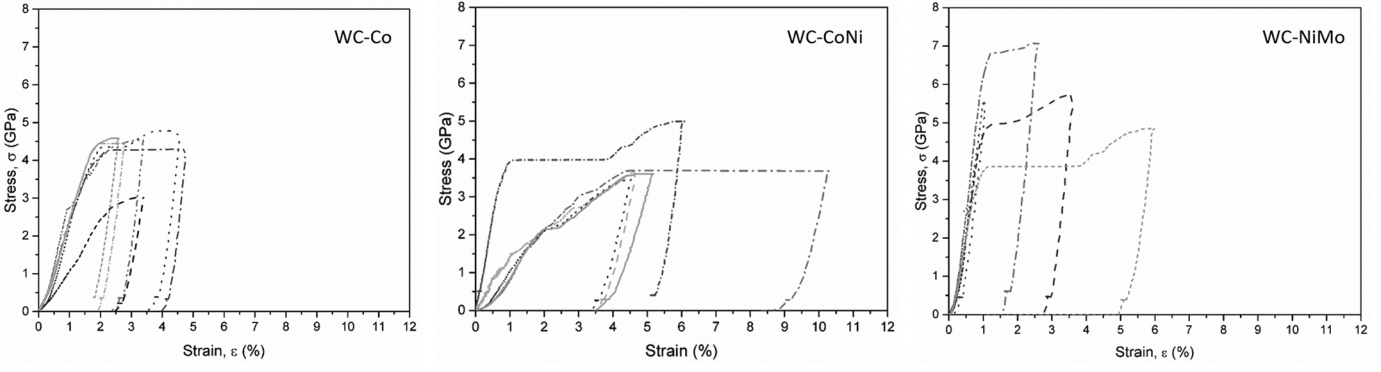
WC-Co
Stress, σ (GPa)
Strain, ε (%)
WC-CoNi
Stress (GPa)
Strain (%)
WC-NiMo
Stress, σ (GPa)
Strain, ε (%)

Figure 2

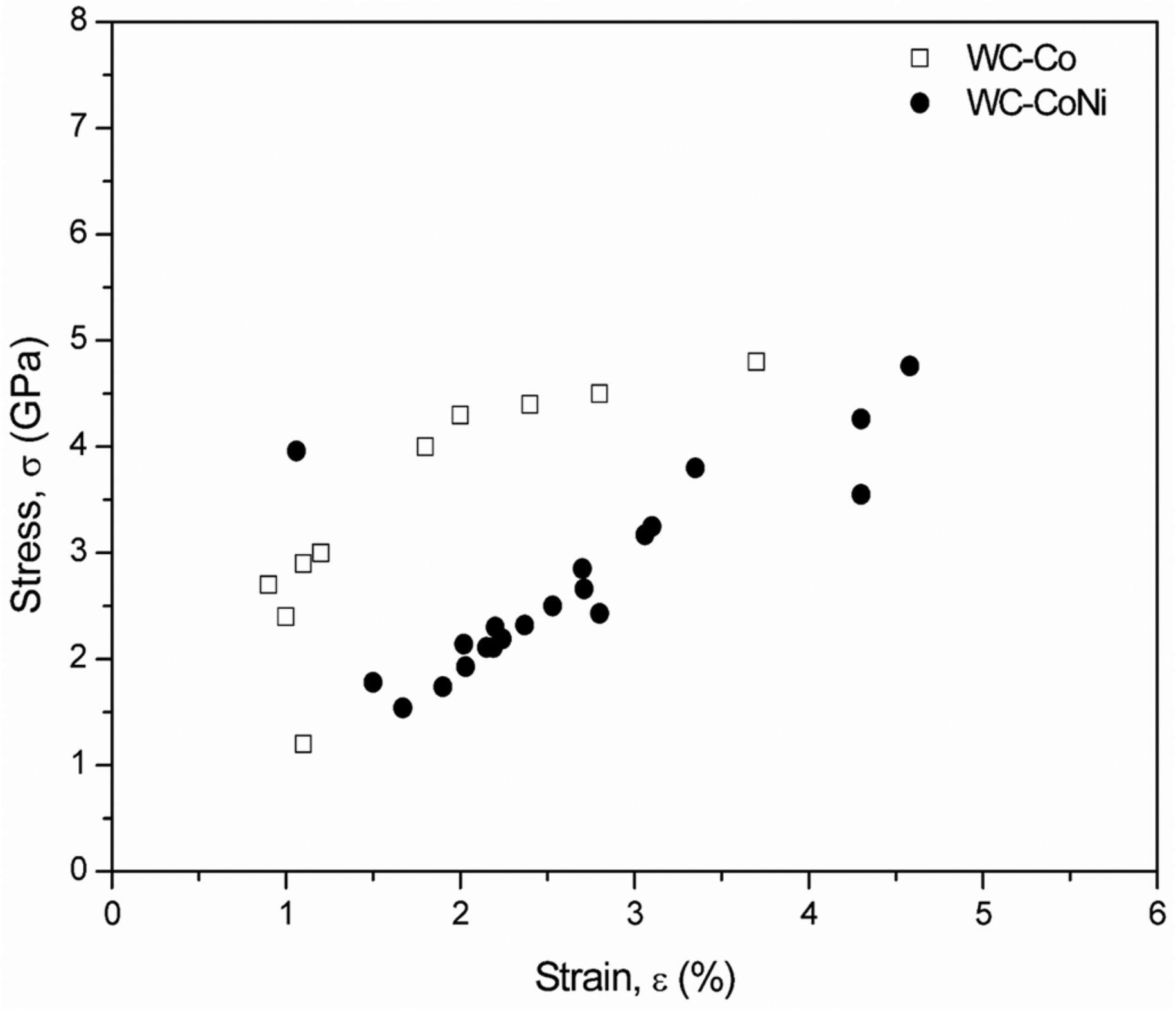

Figure 3

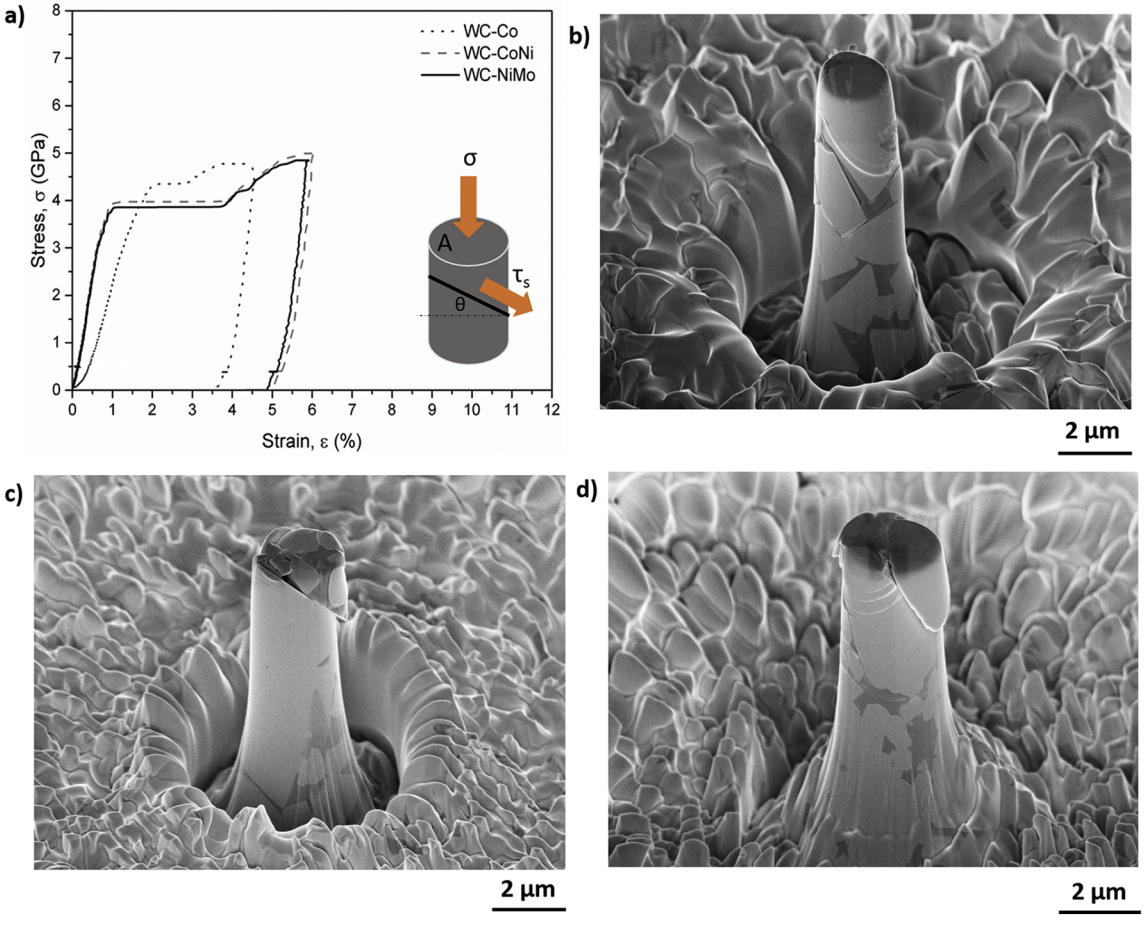
a)
WC-Co
WC-CoNi
WC-NiMo
Stress, σ (GPa)
Strain, ε (%)
σ
A
τs
θ
b)
2 µm
c)
2 µm
d)
2 µm

Figure 4

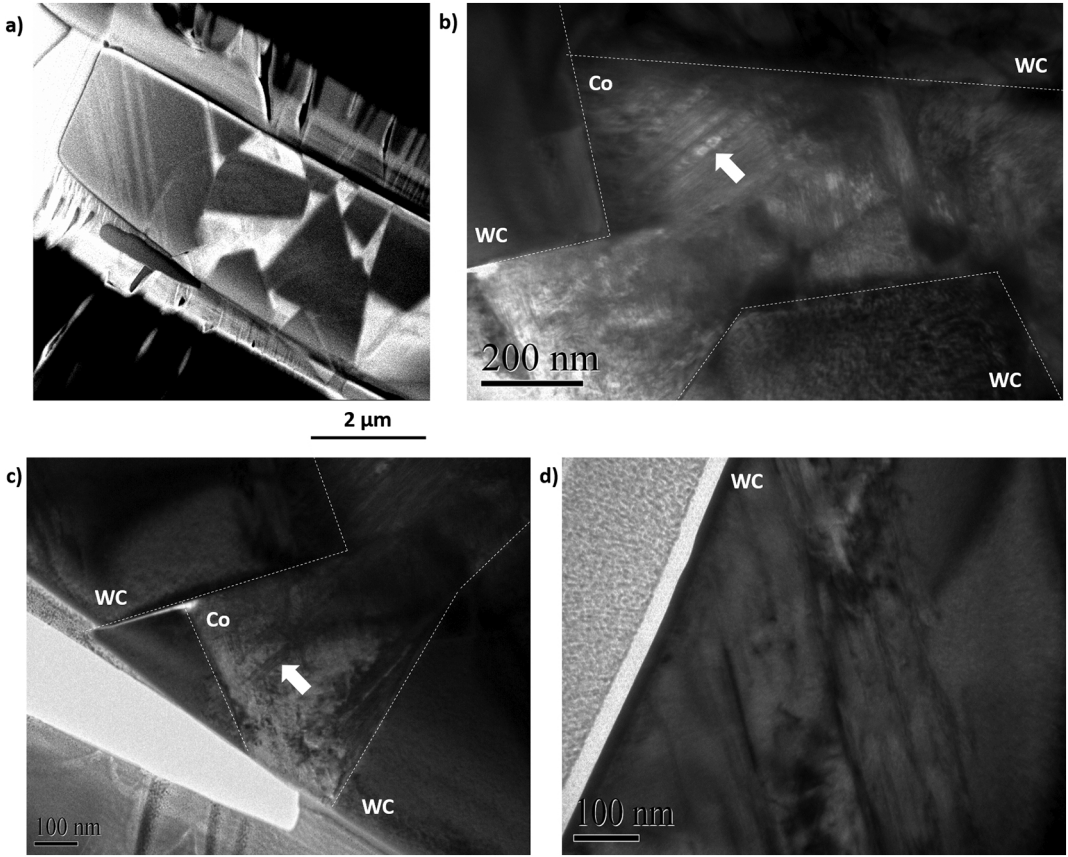

Figure 5

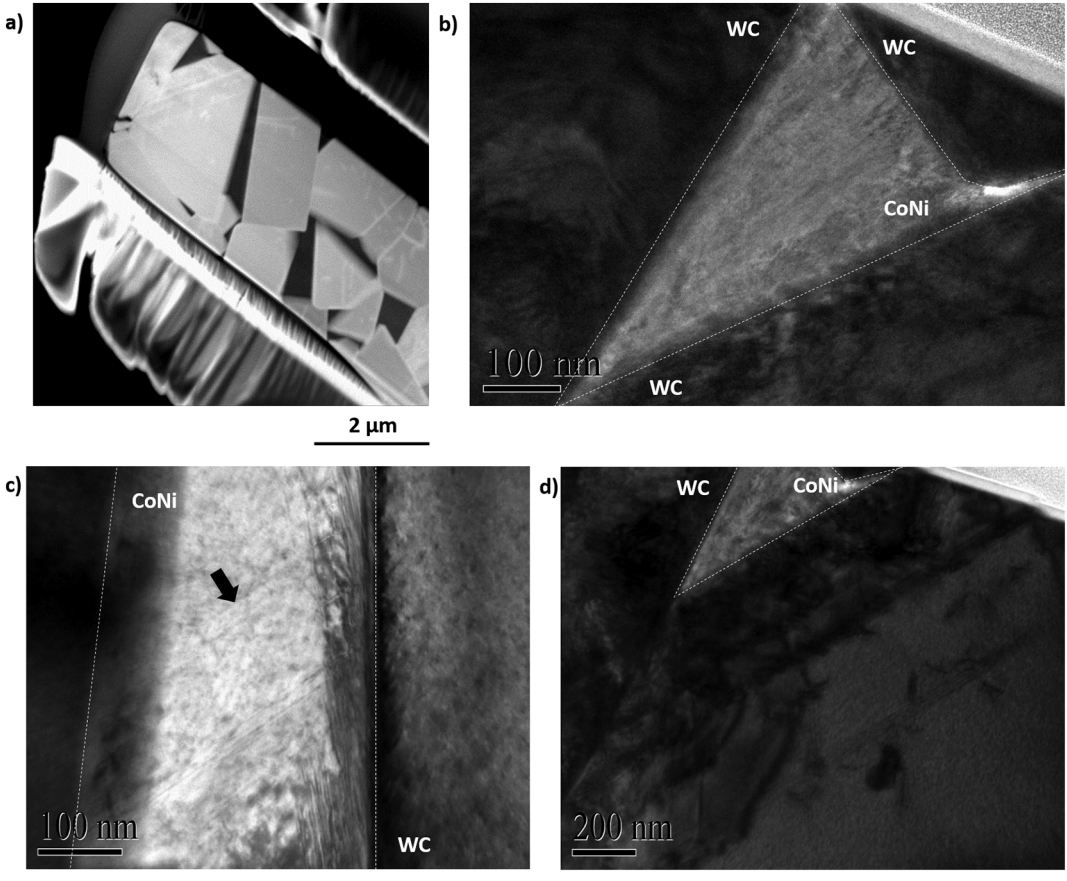

Figure 6

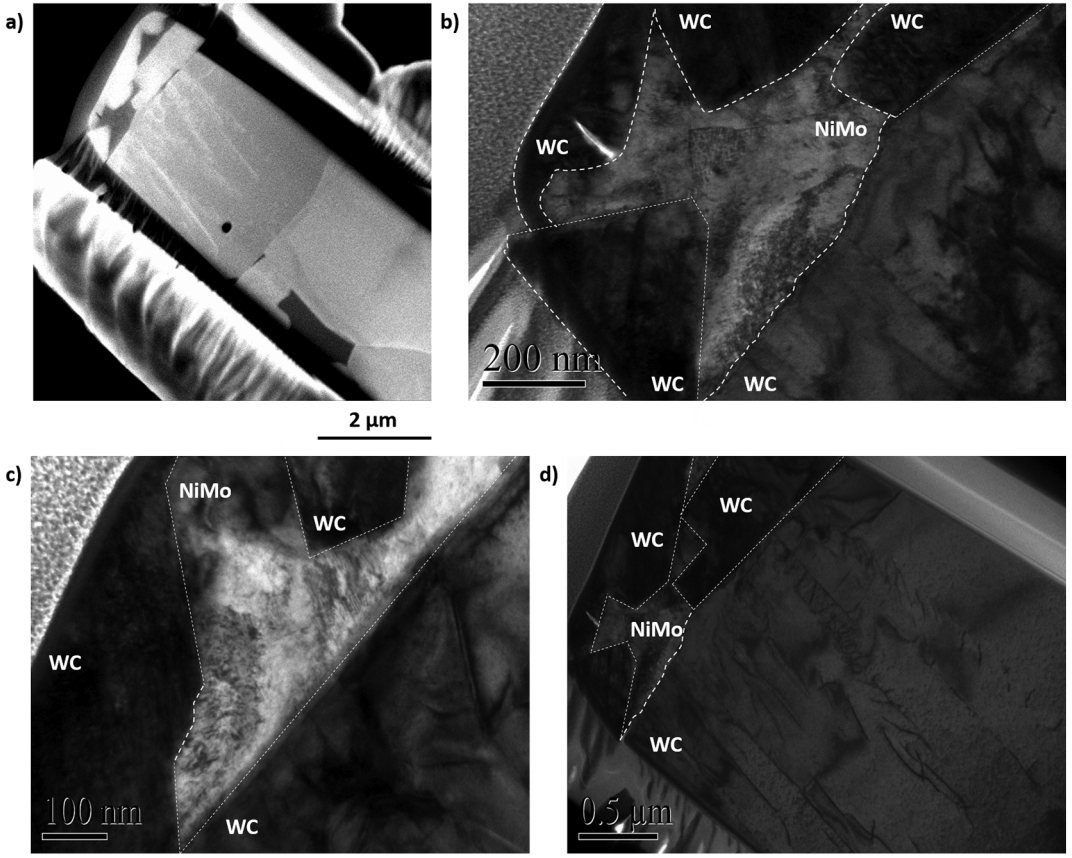
a)
b)
WC
WC
WC
NiMo
200 nm
WC
WC
2 µm
c)
NiMo
WC
WC
100 nm
WC
d)
WC
WC
NiMo
WC
0.5 µm

Figure 7